

Elliptical Galaxies

K.C. Freeman

October 6, 2005

1 Introduction and Goals

Galaxies fall into two main classes: the disks, supported primarily by rotation, and the ellipticals, supported mainly by the random motions of their stars. Dissipation is an important element in the formation of the flat and orderly disk galaxies. On the other hand, it is widely believed that non-dissipative mergers are a major contributor to the formation of at least a large fraction of the giant elliptical galaxies. In these lectures, we will look at the clues about when and how elliptical galaxies formed, and why they have the structural properties that are observed.

2 The Structure of Elliptical Galaxies

2.1 The Radial Light Distribution

Elliptical galaxies show some regularity in the radial light distributions. de Vaucouleurs (1948) proposed a famous empirical law known as the $r^{1/4}$ law, in which the surface brightness distribution is given by the equation

$$I(r) = I_e \exp\{-7.67[(r/r_e)^{1/4} - 1]\}.$$

Here r_e is the radius containing half of the total luminosity (the effective radius) and I_e is the corresponding effective surface brightness. This distribution works very well for many elliptical galaxies, particularly those of intermediate luminosity. Capaccioli *et al.* (1990) showed that the light distribution of the standard elliptical galaxy NGC 3379 is very well represented by the $r^{1/4}$ law over a surface brightness range of about 12 mag. See Figure 1.

The $r^{1/4}$ law is widely used as a representation of spheroidal systems like elliptical galaxies and the bulges of spirals (we will see later how well it works for some bulges). Dynamically, this law is important in our context because it is associated

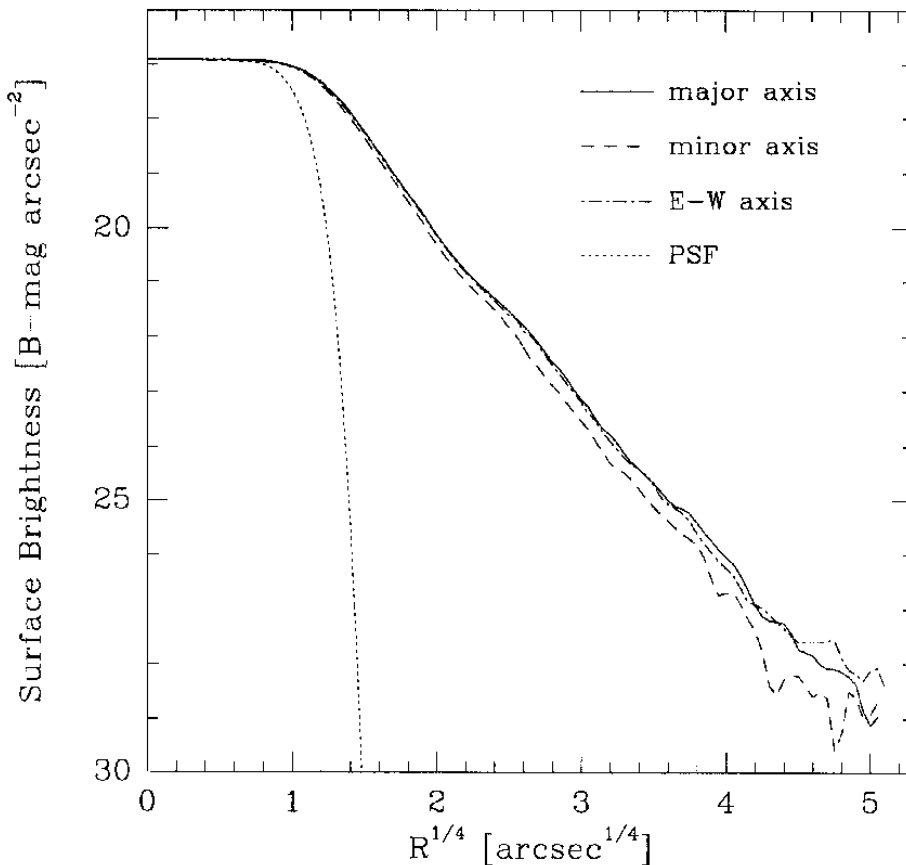


Figure 1: The surface brightness distribution of NGC 3379, showing how well the $r^{1/4}$ law works for this galaxy (from Capaccioli *et al.* 1990)

with violent relaxation processes. van Albada (1982) showed that the outcome of dissipationless collapse with irregular initial conditions and a large collapse factor is well represented by the $r^{1/4}$ law. Similar results were found for the outcome of merging (*e.g.* Barnes 1988) and of tidal stripping (Aguilar & White 1986).

The $r^{1/4}$ law is not such a good fit to all ellipticals. Many authors have shown that there are systematic deviations from the $r^{1/4}$ law and that these deviations are similar for ellipticals of similar luminosities. See Caon *et al.* (1993) for references. A more general fitting function was introduced by Sersic (1968) of the form

$$I(r) = I_0 \exp[-(r/r_0)^n]$$

which corresponds to the $r^{1/4}$ law for $n = 1/4$ and to an exponential law for $n = 1$. This function is now widely used to investigate how the structure of ellipticals changes with absolute magnitude. As n decreases, the surface brightness profile flattens and tends towards a power law of slope -2 .

From the work of Caon *et al.* (1993) and Jerjen *et al.* (1999), for example, it seems

clear now that the $r^{1/4}$ law is just a first approximation to the real situation. The fainter ellipticals have n closer to 1 (the exponential distribution) while the brighter ellipticals may have n even lower than 0.1. The Sersic scale length r_o and the index n vary fairly smoothly with absolute magnitude: see Figure 2. Jerjen *et al.* find that $\log n = 1.4 + 0.10M_B$ where M_B is the absolute blue magnitude. Graham *et al.* (1996) also found a strong decrease of the index n with increasing r_e . (Note that some authors use $1/n$ in place of n).

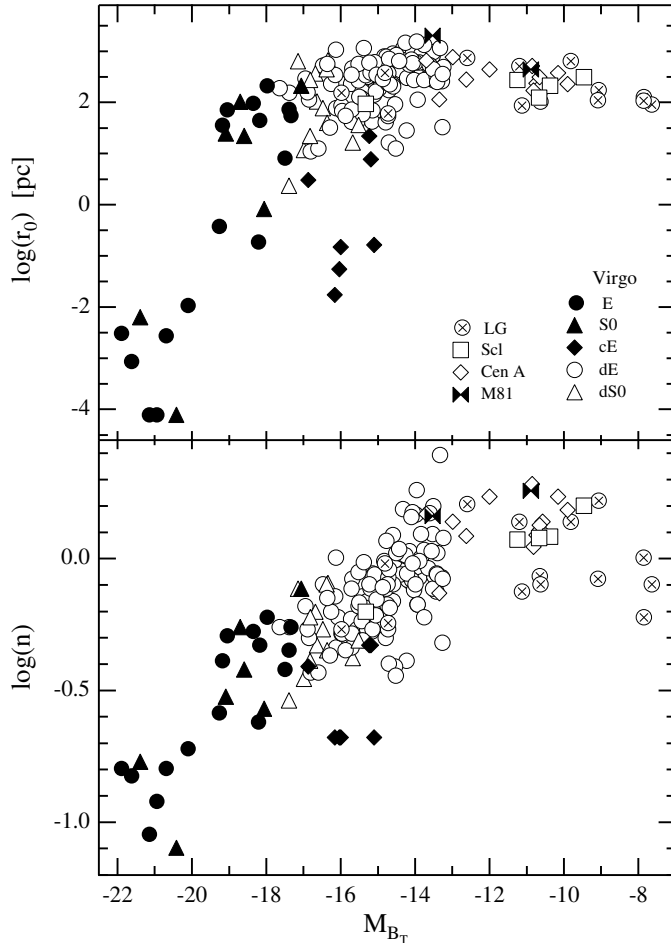


Figure 2: The best fitting Sersic parameters $\log r_o$ (upper) and $\log n$ (lower) as a function of the absorption-corrected absolute B magnitude for early-type galaxies. The $r^{1/4}$ law corresponds to $\log n = -0.60$ (from Jerjen *et al.* (1999)).

I should mention also a simple analytic *volume* density distribution due to Jaffe (1983) that gives a good representation of at least some of the brighter elliptical galaxies. It has the form

$$\rho(r) \propto [r(r + r_J)]^{-2}$$

where r_J is a scale length. For this simple distribution, it is possible to calculate the surface brightness distribution and dynamical quantities like the line-of-sight velocity dispersion, and also the (phase density) distribution function for different dynamical assumptions: see Binney & Tremaine (1987) for more discussion.

2.2 Diskiness and Boxiness

The isophotes of ellipticals are not always elliptical. Some ellipticals show a distinctly boxy structure, while others have a more disk-like appearance. It turns out that the isophote shape is related to the absolute magnitude, to the structure of the innermost parts of the galaxy, and to its gross dynamical properties. See Figure 3.

Boxy galaxies are among the more luminous systems. Their inner regions show cores with a shallow slope in the surface density distribution (see Faber *et al.* 1997; also section 8), and they are flattened primarily by the anisotropy of their velocity dispersion (see section 3). The more disk-like systems are less luminous and typically have a small fraction of their light in faint disks: their spheroidal components are flattened by rotation, and they show a steep cusped density distribution at small radius. Their disks and their spheroidal components are well aligned.

For our purpose, we need to understand the origin of the disk/boxy dichotomy, because it probably relates to the formation processes of massive and less massive ellipticals. Naab *et al.* (1999) have shown that mergers of equal mass disks produce boxy merger products with slow rotation and flattened by anisotropic velocity dispersion, while the mergers of disks with a 3:1 mass ratio produce disk-like systems that are rotationally supported.

3 The Rotation of Ellipticals

The rotation of ellipticals is usefully displayed in a plot of V/σ vs ϵ , where V is the peak rotation of the galaxy, σ its central velocity dispersion and ϵ is a measure of the isophotal ellipticity $\epsilon = 1 - b/a$, where b/a is the isophotal major to minor axis ratio at some isophotal level (typically 25 mag arcsec⁻²). Figure 4 shows a sample of elliptical galaxies from Davies *et al.* (1983). The curve represents the $V/\sigma - \epsilon$ relation for an oblate rotating stellar system with an isotropic velocity dispersion; these systems are flattened by their rotation. Figure 4 shows how the less luminous ellipticals lie close to the oblate isotropic curve, while the brighter ellipticals lie mostly well below it.

The slow rotation of the brighter ellipticals was a major discovery of the late 1970s. The location of the bright ellipticals in the $V/\sigma - \epsilon$ plane indicated that

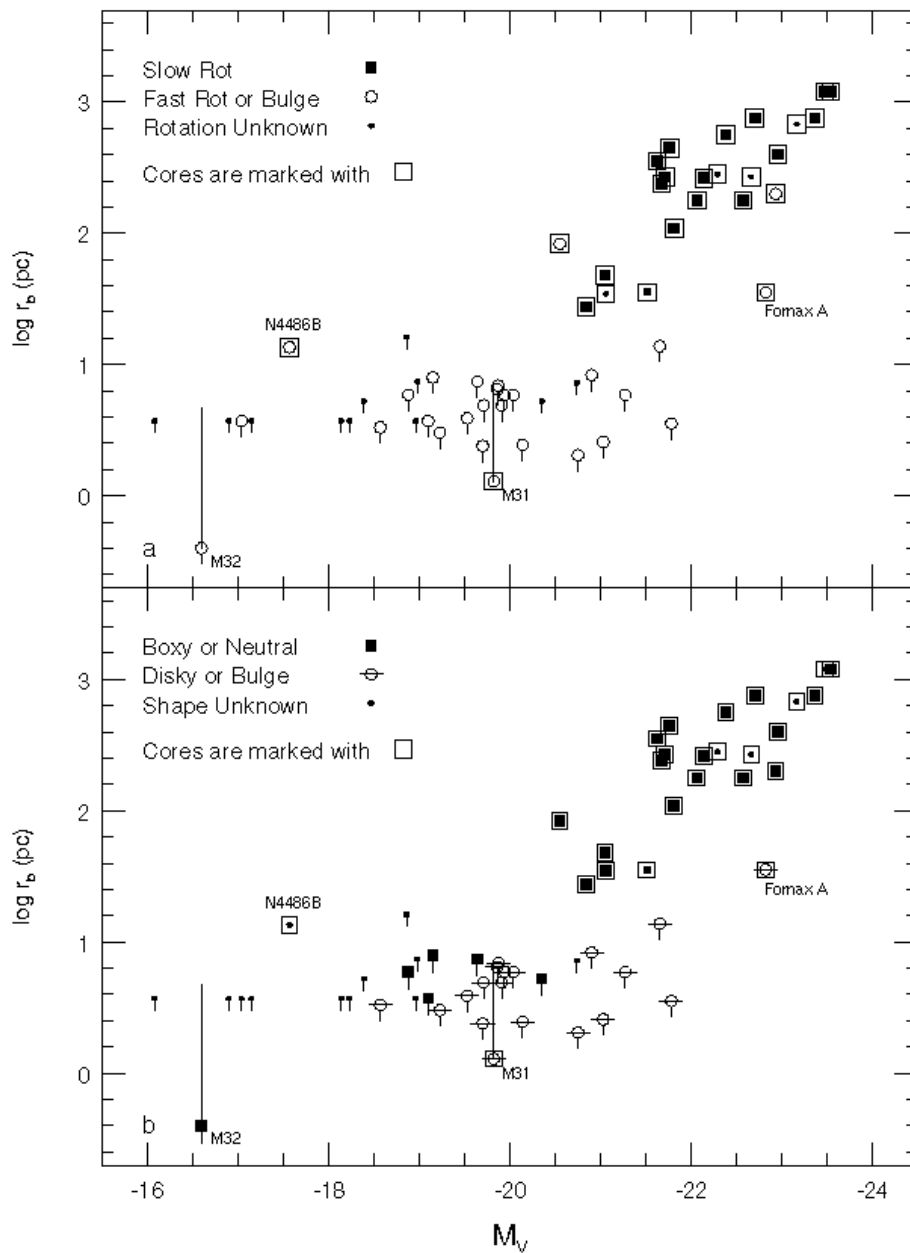


Figure 3: The brighter ellipticals have flatter cores, are slowly rotating and have boxy isophotes. The break radius r_b is the radius at which the core or cusp structure in the inner regions appears. From Faber *et al.* (1997).

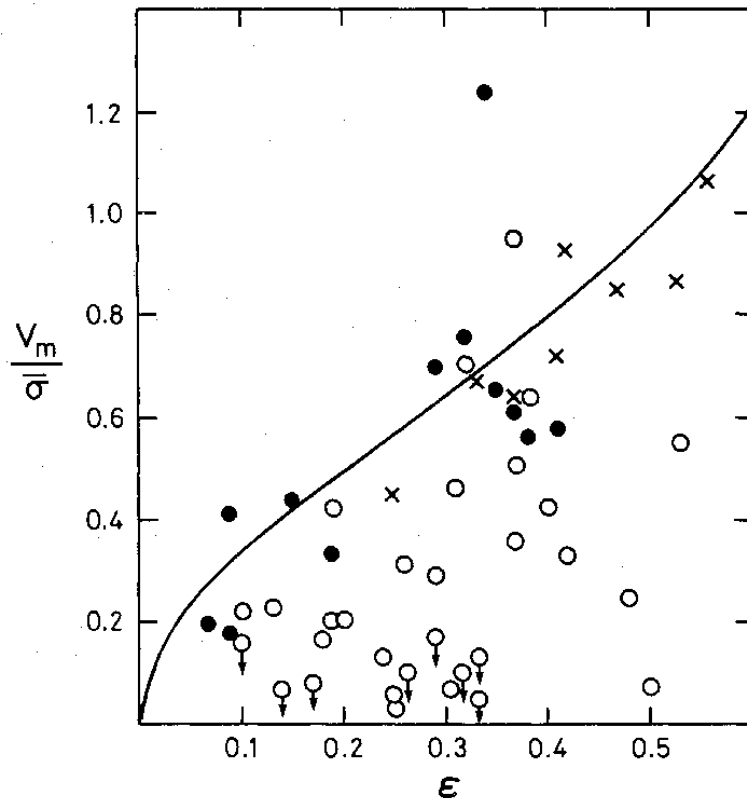


Figure 4: The $V/\sigma - \epsilon$ relation for brighter and fainter elliptical galaxies. The curve shows the locus of oblate rotating stellar systems with an isotropic velocity dispersion. This figure shows how the fainter ellipticals are flattened by rotation, while the brighter ellipticals are flattened by their anisotropic velocity dispersion. Open circles show brighter ellipticals ($M_B < 20.5$), filled circles show fainter ellipticals and crosses show bulges of disk galaxies. (From Davies *et al.* 1983).

these galaxies were flattened by their anisotropic velocity dispersion rather than by rotation. It raised an important problem about the angular momentum of giant ellipticals that was clearly formulated by Fall (1983) in terms of the relationship between specific angular momentum J/M and mass M for spiral and elliptical galaxies. Figure 5 shows a version of the Fall diagram from Zurek *et al.* (1988). The specific angular momentum of the giant ellipticals appears to be about an order of magnitude lower than that of the spirals of similar mass. The different point symbols represent N-body cosmological simulations of the growth of dark halos, scaled to show luminous mass, for dense and less dense environments. Most of the simulated systems lay near the spiral locus, and Zurek *et al.* concluded that the specific angular momentum of the ellipticals had decreased by about an order of magnitude since their formation.

The spectroscopy needed to measure rotation was possible only in the bright inner

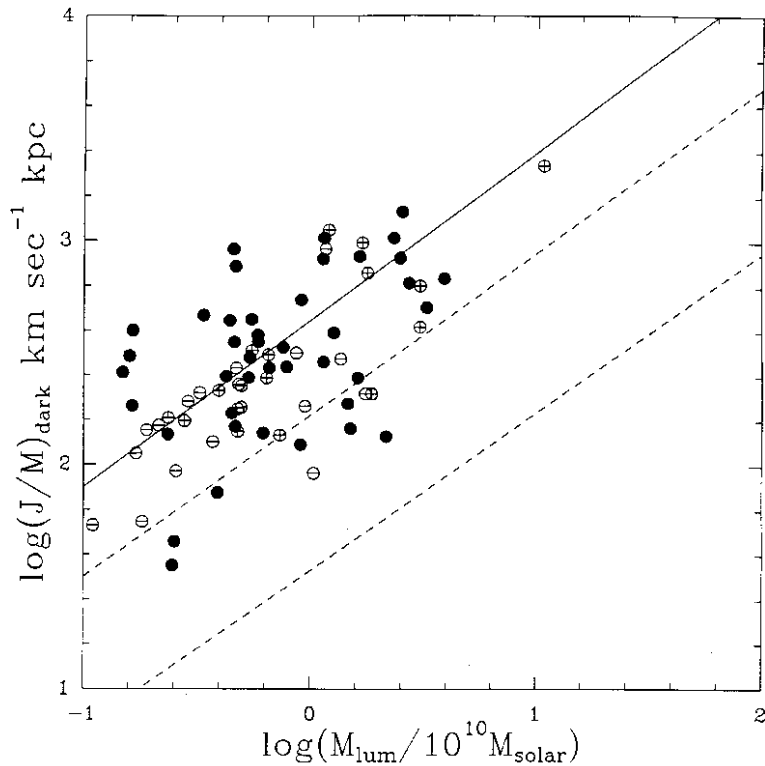


Figure 5: The specific angular momentum J/M vs the mass M for simulated halos, scaled to show luminous mass. The region of the giant ellipticals is represented by the dashed lines, and the locus for spirals is the solid line. The points show $J/M, M$ for simulated systems: see text. (From Zurek *et al.* 1988).

parts of ellipticals, so the region outlined by the dashed lines in Figure 5 shows $J/M, M$ for the *inner* regions of giant ellipticals. Zurek *et al.* argued that angular momentum is transported outwards during the merger processes that build up their halos. Figure 6 shows the evolution of particles from five different bins of binding energy (defined at $z = 0$). The particles that were initially ($z = 5.25$) most bound become more bound and lose angular momentum. The least bound particles become slightly more bound but gain significant amounts of angular momentum through the torques that act during the merging process. In this picture, we would then expect to find a significant amount of angular momentum in the outer parts of these slowly rotating giant ellipticals. Observations of planetary nebulae in the outer regions of several giant ellipticals ($r > 4r_e$) show that this is indeed the situation. Rapid rotation was first detected in the outer parts of Cen A (Hui *et al.* 1995) and then for the more normal giants NGC 1399 and NGC 1316 (Arnaboldi *et al.* 1994, 1998). The total specific angular momentum of giant ellipticals appears to be similar to that of spirals of similar mass, although most of the angular momentum of the giant ellipticals appears to reside at large radius.

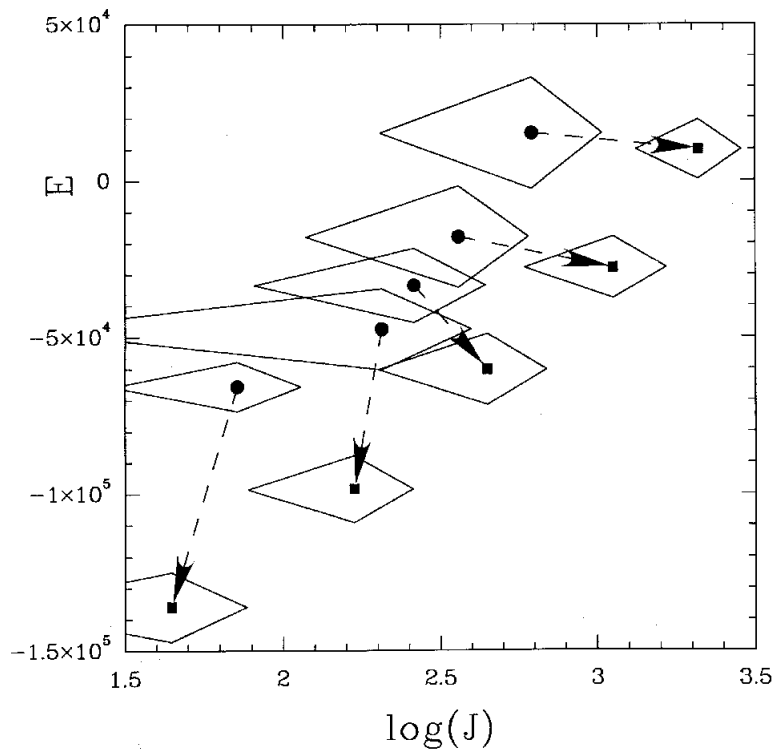


Figure 6: Evolution of a protohalo in the energy-angular momentum plane. At $z = 0$, the halo was partitioned into five bins of binding energy E . The energy and angular momenta of the particles in these bins at $z = 5.25$ (filled circles) were compared with their values at $z = 0$ (filled squares). During the merging processes, angular momentum is transported outwards from the inner regions of the system to the outer envelope (from Zurek *et al.* 1988).

Planetary nebulae kinematics are not yet available for the outer regions of M87, but it seems likely that the angular momentum of M87 again lies mostly in its outer regions. Although the kinematics of globular cluster systems and the main body of the galaxy may be quite different, it is interesting that Cohen *et al.* (1997) find significant rotation in the M87 globular cluster system. The outer parts of M87 are clearly much more elliptical than the inner regions, consistent with a higher angular momentum content. Figure 7 compares an image of M87 from the DSS (limiting surface brightness ~ 24 B mag arcsec $^{-2}$) and a very deep image from Weil *et al.* (1997) (limiting surface brightness ~ 28 B mag arcsec $^{-2}$). This increase of isophotal ellipticity is common among the cluster giant ellipticals; see Porter *et al.* (1991). In summary, we would argue that, although the inner regions of giant ellipticals are flattened primarily by their anisotropic velocity dispersion, the outer regions are flattened mainly by their rotation.

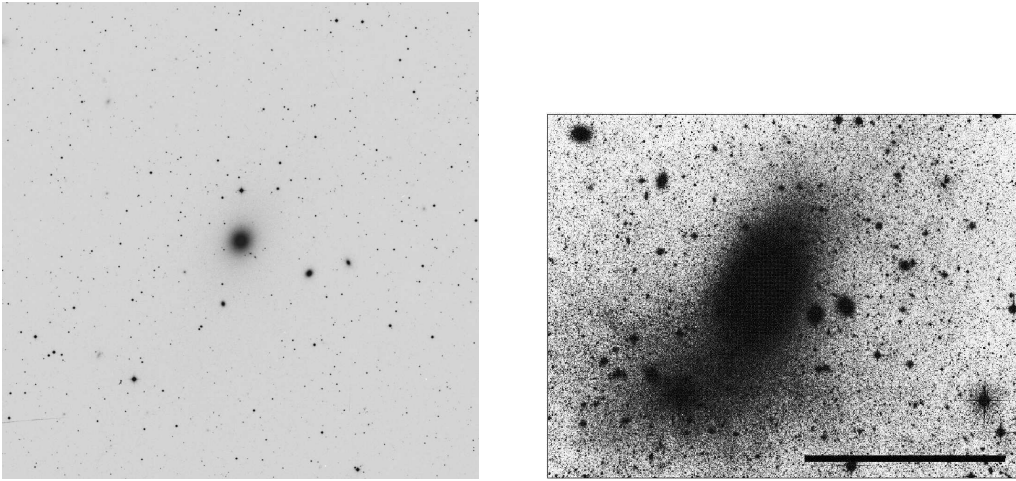


Figure 7: Two images of M87: in the shallow DSS image (left), M87 appears almost round, while in the deep image of Weil *et al.* (1997: right), it is much more elliptical. The two images cover similar regions of sky in the horizontal direction. The flattening at large radius is probably a consequence of the angular momentum of the outer regions.

4 The Fundamental Plane

The fundamental plane is a scaling relation between structural and kinematical parameters for elliptical galaxies. It started with the Faber-Jackson (1976) relation between luminosity and central velocity dispersion; a recent K-band derivation of this law gives $L_K \propto \sigma^{4.14 \pm 0.22}$ (Pahre *et al.* 1998). This law can easily be derived from the virial theorem, if the mean surface brightness and M/L ratio do not vary significantly from galaxy to galaxy. However, it soon became clear that the residuals from this relation correlated with the surface brightness, and the fundamental plane includes this correlation. It is usually presented in the form (*e.g.* Pahre *et al.* 1998)

$$r_e \propto \sigma^A I_e^B$$

where r_e is the effective radius, σ the central velocity dispersion and I_e the mean surface brightness within r_e . The virial theorem gives

$$R \propto V^2 I^{-1} (M/L)^{-1}$$

where R , V^2 and I are suitably defined means of radius, internal velocity and surface brightness. If M/L is constant, and the galaxies are homologous, *i.e.* $r_e \propto R$, $\sigma^2 \propto V^2$ and $I_e \propto I$, then the virial theorem corresponds to

$$r_e \propto \sigma^2 I_e^{-1}.$$

The parameter A depends strongly on the observed wavelength, changing from about 1.0 at U through 1.25 at B to 1.5 at K. In the K-band, where line blanketing effects on the M/L ratio are reduced, the observed fundamental plane for elliptical galaxies has the form (Pahre *et al.* 1998)

$$r_e \propto \sigma^{1.53 \pm 0.08} I_e^{-0.79 \pm 0.03}$$

with a scatter of about 0.096 in $\log r_e$. See Figure 8.

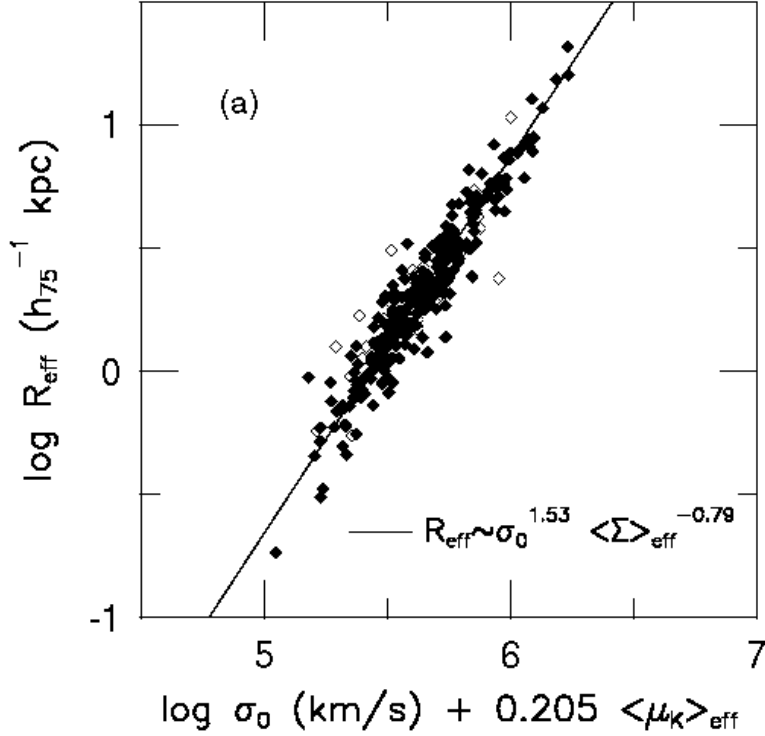


Figure 8: The K-band fundamental plane for 251 early-type galaxies, from Pahre *et al.*(1998), seen edge-on along its long side.

This departure from the virial theorem scaling (*i.e.*the *tilt* of the fundamental plane) can be produced by a systematic change of M/L with mass, due to stellar population changes with mass (*e.g.* mean age, metallicity, IMF), or to a change in the dark/luminous mass ratio within r_e : the K-band tilt corresponds to the relation $M/L \propto M^{0.16 \pm 0.01}$. Alternatively, this tilt of the fundamental plane could come from a systematic breakdown of the homology assumption, such as changes with mass in the shape of $I(r)$ and $\sigma(r)$, and in rotation and kinematic anisotropy. For example, we know already that the brighter ellipticals are more anisotropic and have shallower $I(r)$ distributions. Graham & Colless (1997) show

how correcting for broken homology can bring the exponents of σ and I_e in the fundamental plane closer to the virial theorem values. Busarello *et al.* (1997) find that non-homology in the dynamical structure of ellipticals accounts for more than half of the tilt of the fundamental plane. The scatter about the fundamental plane cannot be accounted for by observational errors alone. Small variations in age, metallicity and non-homology at any point along the fundamental plane probably contribute to the observed scatter.

The globular clusters in our Galaxy illustrate the homology problem nicely (Djorgovski 1995). Within the cores of the clusters, the structure and M/L ratios are fairly similar from cluster to cluster. The fundamental plane for the cores of globular clusters has the form

$$r_c \propto \sigma^{1.8 \pm 0.15} I_o^{-1.1 \pm 0.1}$$

which is close to the virial theorem scaling. On the other hand, at the half-light radius r_h , the M/L ratio is still fairly similar but the dissimilarities in structure from cluster to cluster (i.e. the variations in the ratio of r_t/r_c) are already well established: the corresponding fundamental plane is

$$r_h \propto \sigma^{1.45 \pm 0.2} I_h^{-0.85 \pm 0.1}$$

(here σ is still the central velocity dispersion), which is similar to the observed K-band fundamental plane for the elliptical galaxies.

Whatever the reason for the deviation of the fundamental plane from the virial theorem scaling, the intrinsic scatter about the fundamental plane for elliptical galaxies is small, despite the wide range in the rotation parameter (V/σ), and the different $I(r)$ and $\sigma(r)$ profiles, etc. So the departures from constant M/L and/or homology are well organised to keep the fundamental plane tight. This needs explaining. It may be an indication that elliptical galaxies can attain only a restricted subset of dynamical possibilities via their formation processes (violent relaxation, mergers . . .)

Although the fundamental plane does not include metallicity as one of the variables, there is an important relationship between the metallicity and the luminosity, which is often expressed as an $Mg_2 - \sigma$ relation, because Mg_2 (a measure of the strength of the Mg b feature) and σ are distance-independent. In this form, it represents an increase of metallicity with deepening potential well: see Figure 9.

With the assumption of homology, the tilt of the fundamental plane can be interpreted as a relationship between the M/L ratio and mass or luminosity. For example, Mobasher *et al.* (1999) find that $M/L \propto M^{0.18 \pm 0.01}$ at K and $M/L \propto M^{0.23 \pm 0.01}$ at optical wavelengths. This is usually interpreted as coming from the mass-metallicity relation.

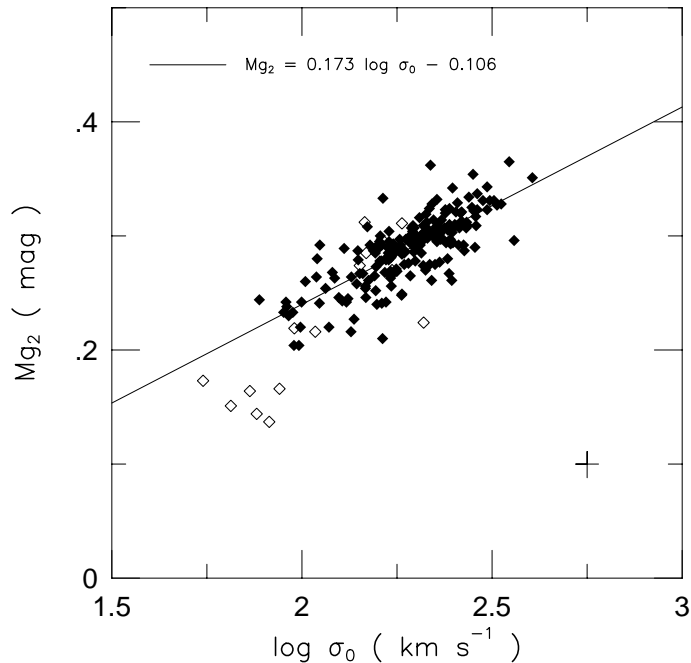


Figure 9: The $Mg_2 - \sigma$ relation for 182 galaxies, from Pahre *et al.* (1998).

The fundamental plane at higher redshifts gives constraints on the evolution of M/L and the epoch of star formation in ellipticals, if the assumption of homology remains correct. Evolutionary effects on M/L have been derived out to redshifts of about 0.8. For example, van Dokkum *et al.* (1998) used fundamental plane arguments to derive the evolution of M/L from clusters with redshifts between 0.02 and 0.83; their M/L corresponds to a common rest wavelength near B. Relative to the Coma cluster, they find that $\Delta \log M/L = (-0.40 \pm 0.04)z$ if $\Omega_m = 0.3$. Comparison with population synthesis models gives constraints on the formation epoch and the value of Ω_m : their data favor high formation redshifts and low Ω_m (see Figure 10).

5 [Mg/Fe] in Elliptical Galaxies

In the previous section, we have already seen that the metallicity, as measured by the Mg_2 index, increases with increasing luminosity or velocity dispersion. This is usually ascribed to the ability of galaxies with deeper potential wells to retain chemically enriched material from supernovae. The ratio of alpha elements like magnesium to iron also increases with luminosity: see for example Fisher *et al.*

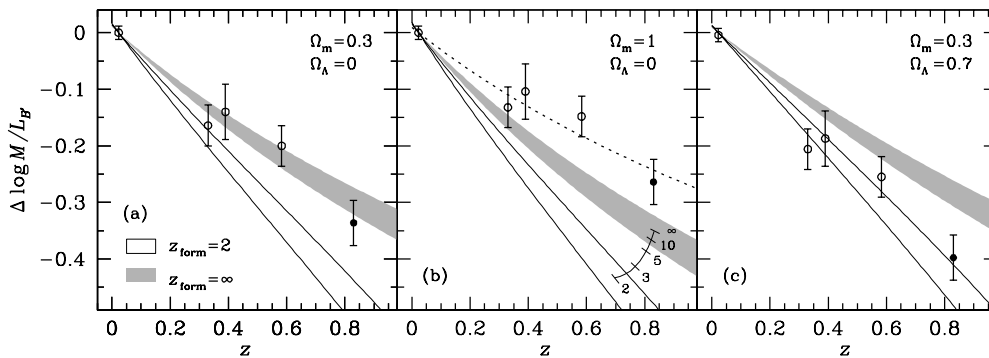


Figure 10: Evolution of M/L with redshift for three cosmological models. Model predictions for different formation redshifts of the stars are shown, assuming a Salpeter IMF ($x = 2.35$) and a range of metallicities. The dotted line in (b) indicates a model with $z_{form} = \infty$ and a steeper IMF ($x = 3.35$). The data favor high formation redshifts and low Ω_m (from van Dokkum *et al.* 1998).

(1995). For the most luminous ellipticals, $[Mg/Fe] \simeq 0.4$, while for the fainter ellipticals, it is close to the solar value. The usual interpretation is that SNI were more significant in the enrichment of the more luminous ellipticals, which in turn suggests that most of the star formation occurred rapidly (within about 1 Gyr) before enrichment by the Fe-producing SNIa could occur.

6 Dwarf Ellipticals

Dwarf elliptical galaxies ($M_B > -18$) fall into two classes: compact systems of high surface brightness, like M32, and diffuse ellipticals of low surface brightness like the nearby dwarf spheroidal galaxies. The Sersic profile index n for a sample of giant and dwarf ellipticals is shown in Figure 2, with the dwarfs having surface brightness profiles that are close to exponential. The apparent continuity of the n - absolute magnitude relation is striking.

The Sersic profile fits by Jerjen *et al.* (1999) give a formal model value for the central surface brightness. Figure 11 shows how this central surface brightness becomes systematically fainter for the fainter ellipticals (except for the compact M32-like systems). Again, the continuity of the surface brightness - absolute magnitude relation is evident, and indicates that these low surface brightness dwarfs are the low luminosity extension of the classical giant ellipticals.

Large numbers of dwarf ellipticals are found in nearby clusters like Virgo, Fornax and Centaurus (Sandage *et al.* 1985, Ferguson & Sandage 1988, Jerjen & Tammann 1997), with their luminosity function rising steeply towards fainter magnitudes. An interesting subclass of brighter dwarf ellipticals have sharp central

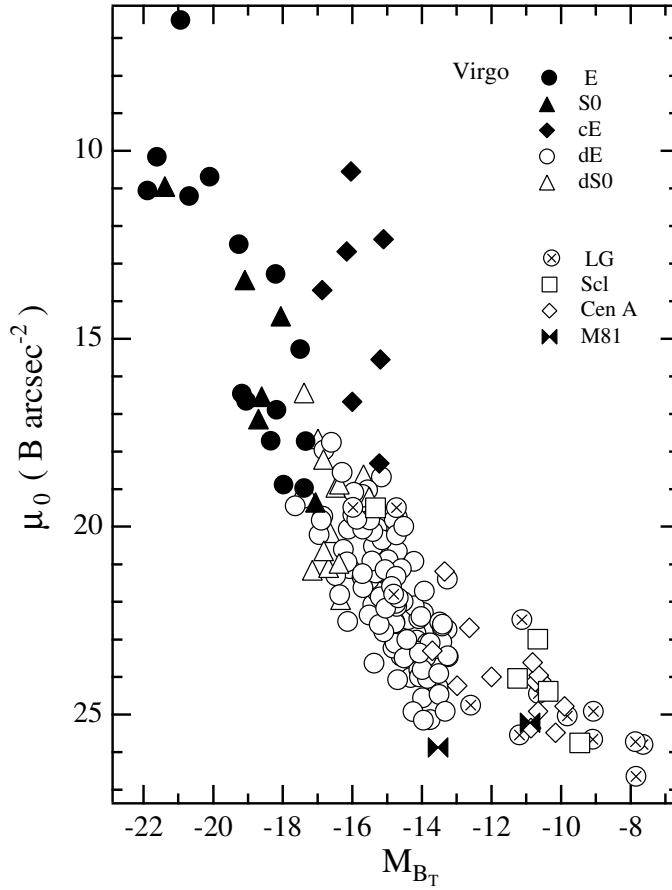


Figure 11: The central surface brightness μ_0 of the best-fitting Sersic model *vs.* the absolute absorption-corrected B magnitude. The galaxies are shown with different symbols according to their type (Virgo) and their group membership. Note the continuity between classical and dwarf early-type galaxies. Brighter galaxies have higher central surface brightnesses (from Jerjen *et al.* 1999).

nuclei. In both the Virgo and Fornax clusters, the nucleated and non-nucleated dwarf ellipticals show different radial distributions within the clusters. The nucleated dwarfs follow the strongly clustered distribution of the bright ellipticals, while the brighter non-nucleated dwarfs ($M_B < -14.2$) are more loosely distributed, like the spirals and dIrr galaxies (see Ferguson & Sandage 1989). This is an important clue to the evolution of galaxies in the potential well of clusters; the reason for the different distributions of nucleated and non-nucleated dwarfs in these clusters is however not yet understood.

The origin of the dwarf ellipticals is also not well understood. Most of the faint nearby dwarf spheroidal galaxies have complex star formation histories (see for example Grebel 1999). Some of these apparently structureless systems were forming stars until ~ 1 Gyr ago, and may well have looked like present-day dIrr or dIrr/dSph transition systems at that time. In clusters of galaxies, the harassment process is likely to be a significant source of dwarf ellipticals. This process transforms many of the lower surface brightness spiral galaxies, which have shallow extended potential wells, into dwarf ellipticals through the combined action of fast binary encounters and the tidal field of the cluster itself. Much of their mass is stripped and now resides in the intracluster medium. Moore *et al.* (1998) note the large numbers of small spirals in clusters at intermediate redshift, and their absence in nearby clusters where dwarf ellipticals comprise most of the faint end of the luminosity function. See also Moore *et al.* (1999).

7 The Formation of Ellipticals

The work of Toomre & Toomre (1972) first demonstrated the likely importance of mergers in forming ellipticals. Now this process is seen also in the context of hierarchical models for structure formation. While the stars of most elliptical galaxies appear to have formed at $z > 2$, the structures of the elliptical galaxies may have formed much later, as shown by the example of the cluster MS1054-03 at $z = 0.83$ in which many dissipationless mergers of early type galaxies are observed. It still seems likely that some ellipticals are formed through the later mergers of already-formed disk galaxies, as Toomre (1977) suggested.

At a more specific level, we recall the recent study by Naab *et al.* (1999) who showed how mergers of equal mass disks produce boxy slowly rotating systems flattened by anisotropy, while mergers of disks with 3:1 mass ratios produce disk systems that are rotationally flattened. We also recall that the surface density distribution of dissipationless merger products can be well represented by the $r^{1/4}$ law.

Some ellipticals appear to have been involved in relatively recent merger or accretion events. The shell systems like NGC 3923 (*e.g.* Quinn 1984) are evidence for a recent accretion of a small stellar system which was drawn in to the parent

galaxy by dynamical friction and then tidally disrupted. Galaxies like Cen A with its minor axis lane of dust and gas and its complex shell system (Malin *et al.* 1983) are probably the product of a recent accretion of a more substantial gas-rich companion.

8 The Inner Regions of Ellipticals

8.1 Surface Photometry

The structure of the innermost regions of ellipticals is closely related to their largescale structure and dynamics. HST surface photometry of the inner few hundred parsecs of a large sample of early-type galaxies (Faber *et al.* 1997) showed that the inner surface brightness distribution follows a power law $I(r) \propto r^{-\gamma}$ where γ lies in the range 0 to 1. It turns out that γ has a bimodal distribution within this range, with γ depending on the luminosity of the galaxy. Figure 12 shows the inner surface brightness profiles for this sample: the bimodal distribution of the slope in the central regions is clear.

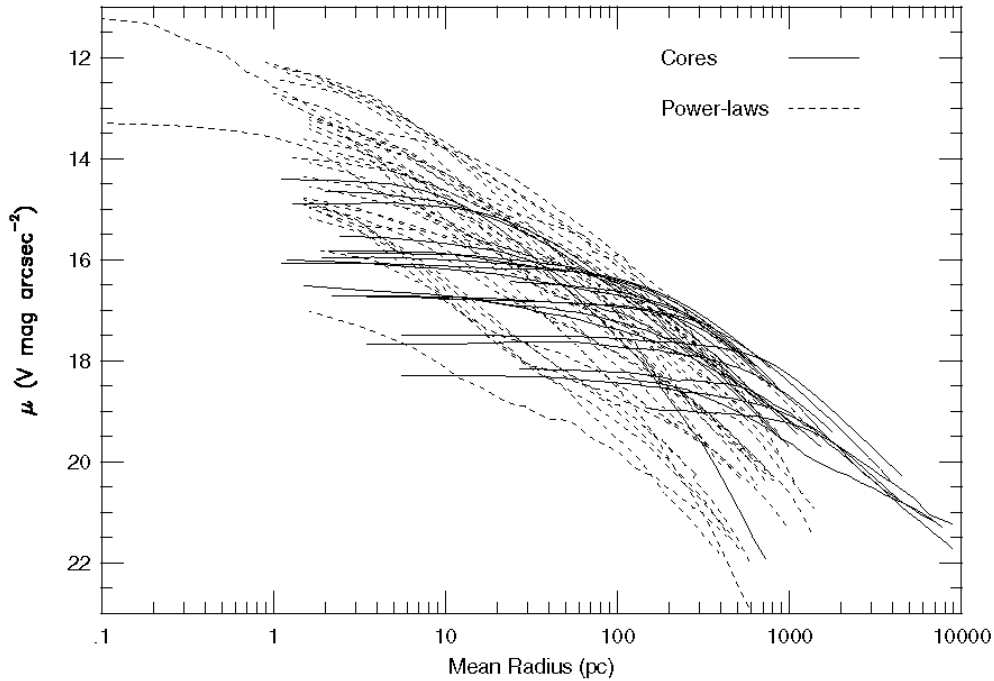


Figure 12: V-band surface brightness profiles of the inner regions of 55 early-type galaxies from HST observations. The dichotomy between the shallow inner power laws (core galaxies: solid lines) and the steeper distributions (power law galaxies: dashed lines) is evident. (from Faber *et al.* 1997).

For the brightest galaxies, with $M_V < -22$, the surface brightness distribution changes slope at the break radius r_b ; within r_b they have flat inner cores with $\gamma < 0.3$. On the other hand, the fainter galaxies, with $M_V > -20.5$, have steep inner cusps with $\gamma = 0.8 \pm 0.3$. Few galaxies have γ values between these two modes. As mentioned already in section 2, most of the more luminous galaxies (low γ) have boxy isophotal shapes, and most of the less luminous galaxies (steep γ) are disk. Remarkably, in the region of intermediate luminosity ($-22 < M_V < -20.5$) where galaxies are found in both of the γ modes, the galaxies with low γ are again boxy systems and the galaxies with steep γ are disk: see Figure 3. Why should there be such a close relationship between the morphology of the innermost 100 pc of early type galaxies and their global boxiness/diskiness which is defined on much larger scales? Before considering this question, we should discuss the central massive dark objects that are detected in most early-type galaxies.

8.2 Central Massive Dark Objects in Early Type Galaxies

Most early-type galaxies appear to have massive dark objects (MDOs) at their centers: is there any connection between these dark objects and the structural properties of the inner parts of these galaxies? Magorrian *et al.* (1998) made dynamical models for a sample of 36 galaxies with HST photometry and ground-based kinematics. They used axisymmetric two-integral models with constant M/L ratio plus the central MDO and found good fits to the structure and kinematics for 32 of their galaxies. The dependence of the derived M/L ratios for the underlying galaxies on the galaxy luminosity is similar to that found from fundamental plane arguments (section 4): $M/L \propto L^{0.2}$. For most of their sample, the data are consistent with a gaussian distribution of $\log M_\bullet/M_{\text{bulge}}$ (where M_\bullet is the mass of the MDO), with a mean of -2.28 and a standard deviation of 0.51 : *i.e.* with a typical value of $M_\bullet/M_{\text{bulge}} \simeq 0.005$. See Figure 13.

The correlation of M_\bullet with M_{bulge} is not particularly tight. In a striking development, it was found that the black hole mass M_\bullet correlates much more tightly with the velocity dispersion of the bulge $\sigma(r_e)$ as measured at the effective radius r_e of the bulge. (Gebhardt *et al.* 2000; Ferrarese & Merritt 2000). The dispersion within r_e is a good measure of the typical dispersion of the bulge itself (*i.e.* in the absence of the black hole). Figure 14 compares the two correlations. The tight $M_\bullet - \sigma$ relation relates the mass of the black hole to the depth of the potential well of the bulge itself.

The implication is still obscure. It may just reflect a tight correlation between the black hole mass and the bulge mass, which was obscured by inaccurate estimates of the bulge mass: *i.e.* the velocity dispersion alone may be a more accurate estimator of the bulge mass. This does not seem very plausible, because we have seen already in §4 that ellipticals are two-parameter systems. Alternatively the

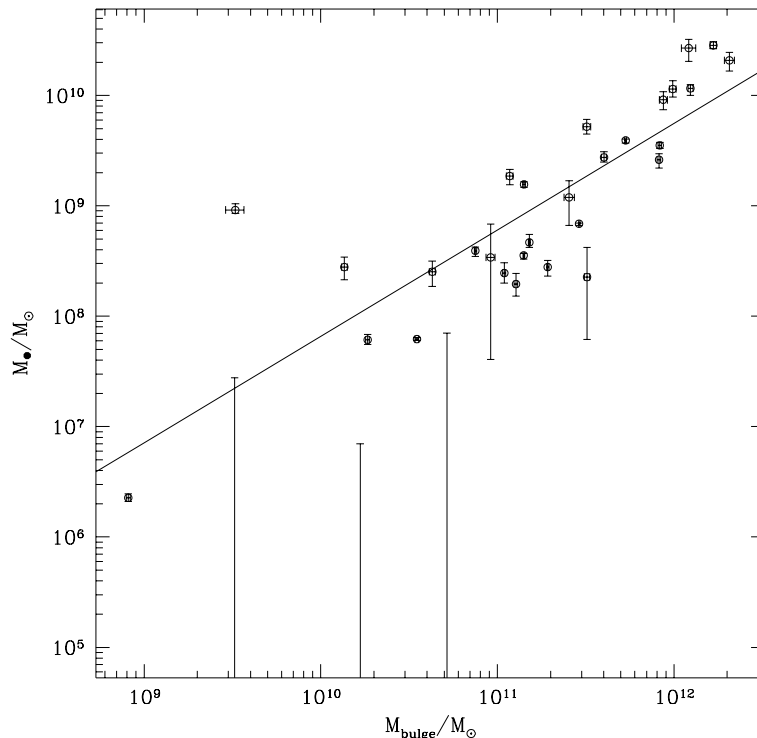


Figure 13: Correlation between MDO mass M_{\bullet} and galaxy mass M_{bulge} . The aberrant point is NGC 4486B, a low luminosity galaxy which has the velocity dispersion and metallicity of a much brighter galaxy. The solid line shows the fit $\log M_{\bullet}/M_{\text{bulge}} = -1.79 - 0.04 \log M_{\text{bulge}}$ (from Magorrian *et al.* 1998).

depth of the potential well of the bulge may somehow define the mass of the black hole that can grow through accretion of stars in the galaxy. See for example Zhao *et al.* (2002).

8.3 Black Holes and the Inner Structure of Early Type Galaxies

The presence of a steep inner density cusp in an early type galaxy is not necessarily associated with a central MDO or black hole. For example the singular isothermal sphere is a simple equilibrium system with a density distribution $\rho(r) \propto r^{-2}$ and no central point mass. In projection, it has a surface density $\propto r^{-1}$, close to what is observed for the cuspy ellipticals. Also, simulations of hierarchical galaxy formation consistently produce dark halos with central cusps at least as steep as $\rho(r) \propto r^{-1}$ (*e.g.* Navarro *et al.* 1996). Nevertheless, there is the possibility that the density cusps and the central black holes are associated.

Several authors have discussed the formation of stellar cusps by the slow growth of a black hole in a pre-existing core. However Merritt (1999) argues that it is

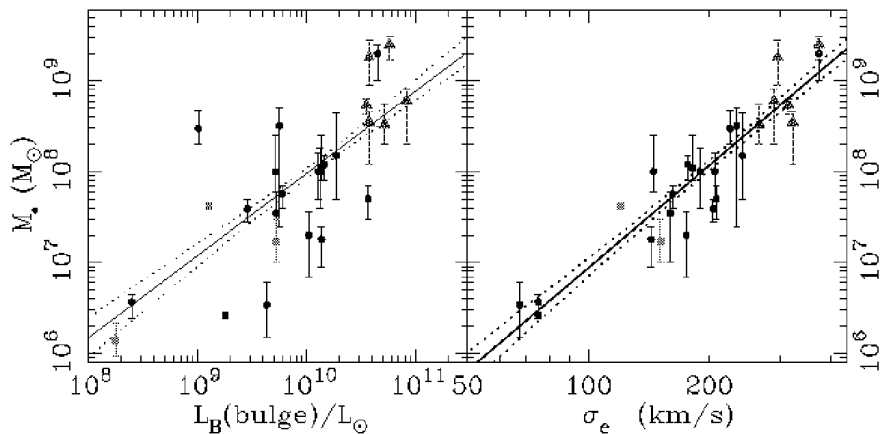


Figure 14: The *left* panel shows the black hole mass against the luminosity of the bulge for 26 early-type galaxies. The *right* panel shows the black hole mass against the luminosity weighted velocity dispersion within an effective radius. The solid line is the best fit correlation and the dotted lines are the 68% confidence limits (From Gebhardt *et al.* 2000).

probably not realistic to consider the growth of a black hole in an initial isothermal sphere with a large core radius, because simulations of violent relaxation tend to produce systems that are already cusped. The growth of a black hole in such a cusped system would give a yet steeper cusp. The shallow cusps of the bright ellipticals are then more difficult to understand in this adiabatic model. An alternative picture for the central regions of these bright ellipticals is through the coalescence of two black holes following a merger of two galaxies, which would transfer energy from the binary black holes to the stars in the inner regions (see for example Makino & Ebisuzaki 1996). This process creates a shallow core with mass comparable to the mass of the black holes. The break radius r_b is then the scale of the region affected by the binary black hole.

References

- Aguilar, L., White, S. 1986. ApJ 307, 97.
 Arnaboldi, M. *et al.* 1994. ESO Messenger, 76, 40.
 Arnaboldi, M. *et al.* 1998. ApJ 507, 759.
 Ashman, K. & Zepf, S. 1992. ApJ 384, 50.
 Barnes, J. 1988. ApJ 331, 699.
 Binney, J., Tremaine, S. 1987. Galactic Dynamics (Princeton:PUP).
 Bower, R., Lucey, J., Ellis, R. 1992. MNRAS 254, 601.
 Busarello, G., Capaccioli, M., Capozziello, S., Longo, G., Puddu, E. 1997. A&A, 320, 415.

Caon, N., Capaccioli, M., D’Onofrio, M. 1993. MNRAS 265, 1013.
 Capaccioli, M., Held, E., Lorenz, H., Vietri, M. 1990. AJ 99, 1813.
 Cohen, J., Ryzhov, A. 1997. ApJ 486, 230.
 Davies, R. *et al.* 1983. ApJ 266, 41.
 de Vaucouleurs, G. 1948. Ann. Astrophys. 11, 247.
 Djorgovski, S. 1995. ApJ 438, L29.
 Dressler, A. *et al.* 1997. ApJ 490, 577.
 Faber, S. *et al.* 1997. AJ 114, 1771.
 Faber, S. & Jackson, R. 1976. ApJ 204 668.
 Fall, S.M. 1983. In Internal Kinematics and Dynamics of Galaxies, (IAU Symposium 100) (Dordrecht: Reidel), p 391.
 Ferguson, H. & Sandage, A. 1988. AJ 96, 1520.
 Ferguson, H. & Sandage, A. 1989. ApJ 346, L53.
 Ferrarese, L. & Merritt, D. 2000. astro-ph/0006053.
 Fisher, D., Franx, M., Illingworth, G. 1995. ApJ 448 119.
 Forbes, D., Brodie, J., Grillmair, C. 1997. AJ 113, 1652.
 Gebhardt, K. *et al.* 2000. astro-ph/0006289.
 Graham, A., & Colless, M. 1997. MNRAS 287, 221.
 Grebel, E. 1999. In “The Stellar Content of Local Group Galaxies”, (ASP), p 17.
 Hui, X., Ford, H., Freeman, K., Dopita, M. 1995. ApJ 449, 592.
 Jaffe, W. 1983. MNRAS 202, 995.
 Jerjen, H., Binggeli, B., Freeman, K. 1999. AJ, in press.
 Jerjen, H. & Tammann, G. 1997. A&A 321, 713
 Kauffmann, G. 1996. MNRAS 281, 487.
 Kodama, T., Arimoto, N., Barger, A., Aragon-Salamanca, A. 1998. A&A, 334, 99.
 Kuntschner, H. & Davies, R. 1998. MNRAS 295 L29.
 McLaughlin, D. 1999. AJ 117, 2398.
 Makino, J. & Ebisuzaki, T. 1996. ApJ 465, 527.
 Malin, D., Quinn, P., Graham, J. 1983. ApJ 272 L5.
 Merritt, D. 1999. astro-ph/9906047.
 Mobasher, B., Guzman, R., Aragon-Salamanca, A., Zepf, S. 1999. MNRAS 304, 225.
 Moore, B., Lake, G., Katz, N. 1998. ApJ 495, 139.
 Moore, B., Lake, G., Quinn, T., Stadel, J. 1999. MNRAS 304, 465.
 Naab, T., Burkert, A., Hernquist, L. 1999. astro-ph/9908129.
 Navarro, J., Frenk, C., White, S. 1996. 462, 563.
 Ohta, K. *et al.* 1996. Nature 382, 426.
 Pahre, M., de Carvalho, R., Djorgovski, S. 1998. AJ 116 1606.
 Porter, A., Schneider, D., Hoessel, J. 1991. AJ 101, 1561.
 Quinn, P. 1984. ApJ 279, 596.
 Sandage, A., Binggeli, B., Tammann, G. 1985. AJ 90, 1759.
 Schweizer, F. 1987. In “Nearly Normal Galaxies” (Springer), p 18.

- Sersic, J. 1968. Atlas de Galaxias Australes. Observatorio Astronomico, Cordoba.
- Taniguchi, Y., Trentham, N., Ikeuchi, S. 1999. astro-ph/9909170.
- Toomre, A. & Toomre, J. 1972. ApJ 178, 623.
- Toomre, A. 1977. In “The Evolution of Galaxies and Stellar Populations” (Yale University Press), p 401.
- van Albada, T. 1982. MNRAS 201, 939.
- van Dokkum, P., Franx, M., Kelson, D., Illingworth, G. 1998. ApJ 504, L17.
- van Dokkum, P., Franx, M., Fabricant, D., Kelson, D., Illingworth, G. 1999. ApJ 520, L95.
- van der Marel, R. 1999. AJ 117, 744.
- Weil, M., Bland-Hawthorn, J., Malin, D. 1997. ApJ 490, 664
- Whitmore, B. *et al.* 1999. astro-ph/9907430.
- Zepf, S. *et al.* 1999. astro-ph/9904247.
- Zurek, W., Quinn, P., Salmon, J. 1988. ApJ 330, 519.